

Open camera or QR reader and scan code to access this article and other resources online.



ORIGINAL ARTICLE

Pump-Free Pneumatic Actuator Driven by the Vapor Pressure at the Gas–Liquid Equilibrium of Aqua Ammonia

Yang Qu,^{1,2,†} Yiming Zhang,^{1,2,†} Boyuan Huang,^{1,2} Cheng Chen,^{1,2} Huacen Wang,^{1,2} Sicong Liu,^{1,2} and Hongqiang Wang^{1–3}

Abstract

Currently, pneumatic soft actuators are widely used due to their impressive adaptability, but they still face challenges for more extensive practical applications. One of the primary issues is the bulky and noisy air compressors required to generate air pressure. To circumvent this critical problem, this work proposes a new type of air pressure source, based on the vapor pressure at the gas–liquid equilibrium to replace conventional air pumps. Compared with the previous phase transition method, this approach gains advantages such as generating gas even at low temperatures (instead of boiling point), more controllable gas output, and higher force density (since both ammonia and water contribute to the gas pressure). This work built mathematical models to explain the mechanism of converting energy to output action force from electrical energy and found the aqua ammonia system is one of the optimal choices. Multiple prototypes were created to demonstrate the capability of this method, including a pouch actuator that pushed a load 20,555 times heavier than its dead weight. Finally, based on the soft actuator, an untethered crawling robot was implemented with onboard batteries, showing the potentially extensive applications of this methodology.

Keywords: artificial muscle, soft actuator, soft robot, untethered robot

Introduction

Soft actuators are an emerging actuation method in the last decades.¹ Unlike traditional electromagnetic motors that use ferromagnetic materials,^{2,3} soft actuators are mainly fabricated through soft materials such as silicone,^{1,4–8} bringing revolutionary improvement in the field of wearable devices, inspection robots, manipulators, and medical robotics,^{9–16} due to their advantages of outstanding adaptability.^{1,4–18} Until

now, many soft actuators have been developed based on numerous mechanisms, such as being driven by fluid pressure, shape memory alloys, ion polymer metal composite, electrostatic adhesion, and dielectric elastomer.^{1,4,19–24} Among them, soft actuators driven by pneumatic pressure are dominant,¹ since air is compressible, safe, and compliant, which is intrinsically adapted to soft actuators, and pneumatic systems have the benefits of low cost, simple design, and high power to weight ratio.²⁵

¹Shenzhen Key Laboratory of Biomimetic Robotics and Intelligent Systems, Department of Mechanical and Energy Engineering, Southern University of Science and Technology, Shenzhen, China.

²Guangdong Provincial Key Laboratory of Human-Augmentation and Rehabilitation Robotics in Universities, Southern University of Science and Technology, Shenzhen, China.

³Southern Marine Science and Engineering Guangdong Laboratory (Guangzhou), Guangzhou, China.

[†]These authors contributed equally to the work.

However, soft pneumatic actuators still face many challenges to more extensive practical applications. One of the primary problems is the air pressure source. Currently, air pressure is usually generated by air compressors, but they are typically heavy, large, and noisy.^{26,27} Air tanks are an alternative, but the operating duration is very limited if the weight and size are constrained.²⁸ Currently, soft robots with pneumatic actuators can hardly move without the air tube from the air pumps, which limits the mobility and extensive applications of soft robotics.

Much effort has been put into removing this barrier, with the heart of the matter is to find an alternative pneumatic source.^{1,12,29,30} Recently, various methods have been proposed, including electrolysis,²⁹ phase transition,^{17,30–32} and chemical reactions,¹² which can generate air pressure from the electrical energy initially stored in batteries to avoid the mechanical movements and components in the conventional air pumps. Previously, various pneumatic soft actuators were implemented based on various fluids (e.g., ethanol). However, there are still imperfections for those phase transition actuators. First, the pressure generated through those liquids is usually low when the temperature is below the boiling point. Thus, most of those actuators use temperatures larger than the boiling point (e.g., 351.5 K for ethanol³⁰). Second, most of those liquids are organic liquids (e.g., ethanol and methanol). Due to the similar solubility properties of the organics and the network properties of soft materials, phase change liquids would dissolve in the soft materials, which can lead to reduced drive capability and limited lifetime.^{17,30–32}

Herein, this article proposes a new type of air pressure source for soft pneumatic actuators—producing gas by heating aqua ammonia. In this system, the chemical reaction for gas, lower solubility to generate gas, and the phase transition of water all happens when the temperature rises, which possesses various advantages compared with the previous purely phase-changing mechanism. First, since this aqua ammonia system reaches a vapor–liquid equilibrium under each temperature, a significant gas pressure difference can be achieved by constantly breaking these equilibrium states through temperature modulation (303–403 K) of Ni–Cr alloy heating wires inside the container. Therefore, pneumatically-driven soft robots can be actuated by the difference in gas pressure generated, regardless of the temperature environment. Second, more gas and pressure can be generated at the same temperature theoretically since the gas comes not only from the phase transition but also from the chemical reaction of ammonia. Compared with the phase transition competitors, aqua ammonia is promising in untethered pump-free soft robotics because it can produce higher gas pressure at a lower temperature with a lower energy consumption cost for the same volume of liquid. Compared with other pneumatic artificial muscles, it has higher force density, as shown in Figure 1A. Moreover, this system is balanced during a large range of temperatures (while phase transition only occurs at the boiling point), which means great controllability.

The contributions of this article are as follows. We propose to integrate aqua ammonia into soft actuators to replace the previous clumsy air pumps to generate air pressure. We build mathematical models to understand the energy conversions and balances (i.e., heat balance, chemical balance, and force

balance) in this system. Then, we implement multiple prototypes to show advantages such as great force/weight ratio and controllability. One of our prototypes can push a load more than 20,555 times heavier than its own weight, which outperforms all of the counterparts,^{4,15,26,30,33–50} as shown in Figure 1A. The velocity and force increase approximately linearly with the electrical input, which can benefit the control of the soft actuator. Finally, we also demonstrate that with these actuators, an untethered soft inchworm robot with an onboard battery can be implemented.

The following section introduces the principle and mathematical analyses. The fabrication and assembly section describes the fabrication procedure of the prototypes. The experimental section characterizes the actuators and demonstrates an untethered robot. Finally, a brief conclusion is drawn.

Modeling and Analyses

To generate the gas and air pressure from aqua ammonia, the mechanism contains four energy forms and three energy conversions in sequence. As shown in Figure 1B, first, the current flows through the heating wire and raises the temperature, and the electric energy is transferred into thermal energy. Then, the heat is conducted into the solution system. Part of the thermal energy is transferred into the chemical energy of aqua ammonia during the decomposition of ammonia monohydrate. Consequently, the ammonia gas is released, increasing the vapor pressure inside the system, and the chemical energy is transferred into the mechanical energy of the vapor–liquid system. The models for these processes are built as follows.

Heat balance

The actuator's energy initially comes from electrical power. The resistance R under the temperature T can be expressed by the following equation:

$$R = R_0(1 + \alpha(T - T_0)), \quad (1)$$

where α is the temperature coefficient of resistance material, and R_0 is the initial resistance at temperature T_0 . If the power is supplied by a DC power supplier, the current can be calculated by Ohm's law:

$$I = U/R, \quad (2)$$

where U is the voltage of the power supplier. According to Joule's law and Fourier's law,⁵¹ the heat generated by the current flowing through the wire can be expressed as follows:

$$Q = I^2 R t, \quad (3)$$

where I is the current flow through the heating wire, R is the resistance of the heating wire, and t is the heat time.

During the phase transition, the heat is divided into three main components, which can be expressed as follows⁵²:

$$Q = Q_l + Q_w + Q_r, \quad (4)$$

where Q_l is the heat loss, Q_w is the heat required to increase the temperature of the aqua ammonia, and Q_r is the heat required to decompose the aqua ammonia.

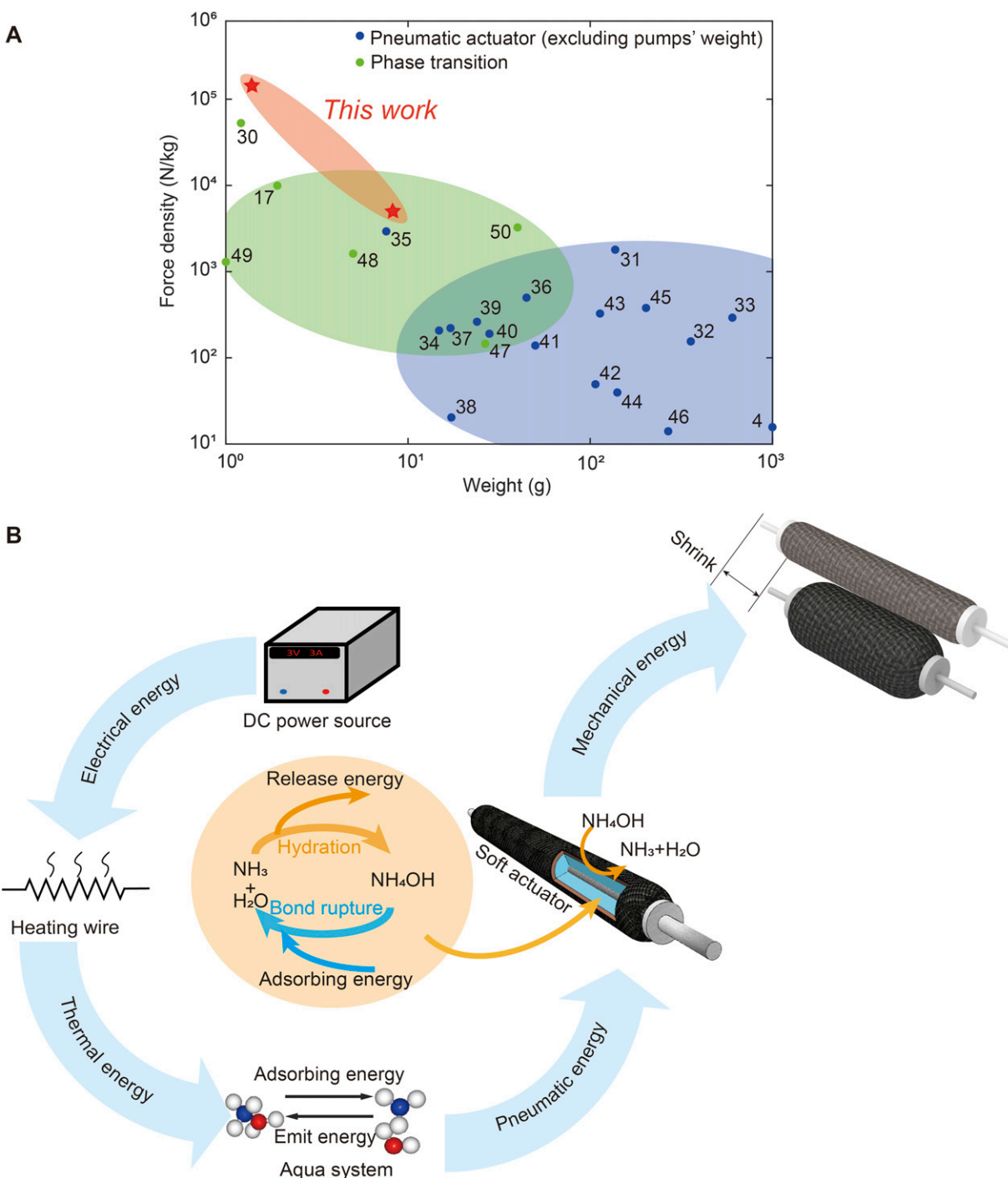


FIG. 1. Basic properties and principle of the artificial muscle driven by the vapor pressure. **(A)** Comparison between the pneumatic actuators driven by the vapor pressure of aqua ammonia and counterparts driven by air pressures generated by pumps and phase transition. **(B)** The energy flow in the artificial muscle is driven by the vapor pressor.

The simplest model of such an actuator is a cylinder. From the center to the outside, there are heating wires, aqua ammonia, and outer rubber. The heat is transferred from the heating wires at the center to the external environment, as shown in Figure 2A. The thermal resistances of the materials can be expressed as follows:

$$\Theta = \sum_{i=1}^4 \Theta_i, \quad (5)$$

where Θ_i is the thermal resistance in the system. The first thermal resistance for the heat convection between the heating wire and aqua ammonia is as follows:

$$\Theta_1 = \frac{1}{h_{ammo} \pi d_{wire}}, \quad (6)$$

where h_{ammo} is the convection heat transfer coefficient of aqua ammonia and d_{wire} is the diameter of the heating wire. The

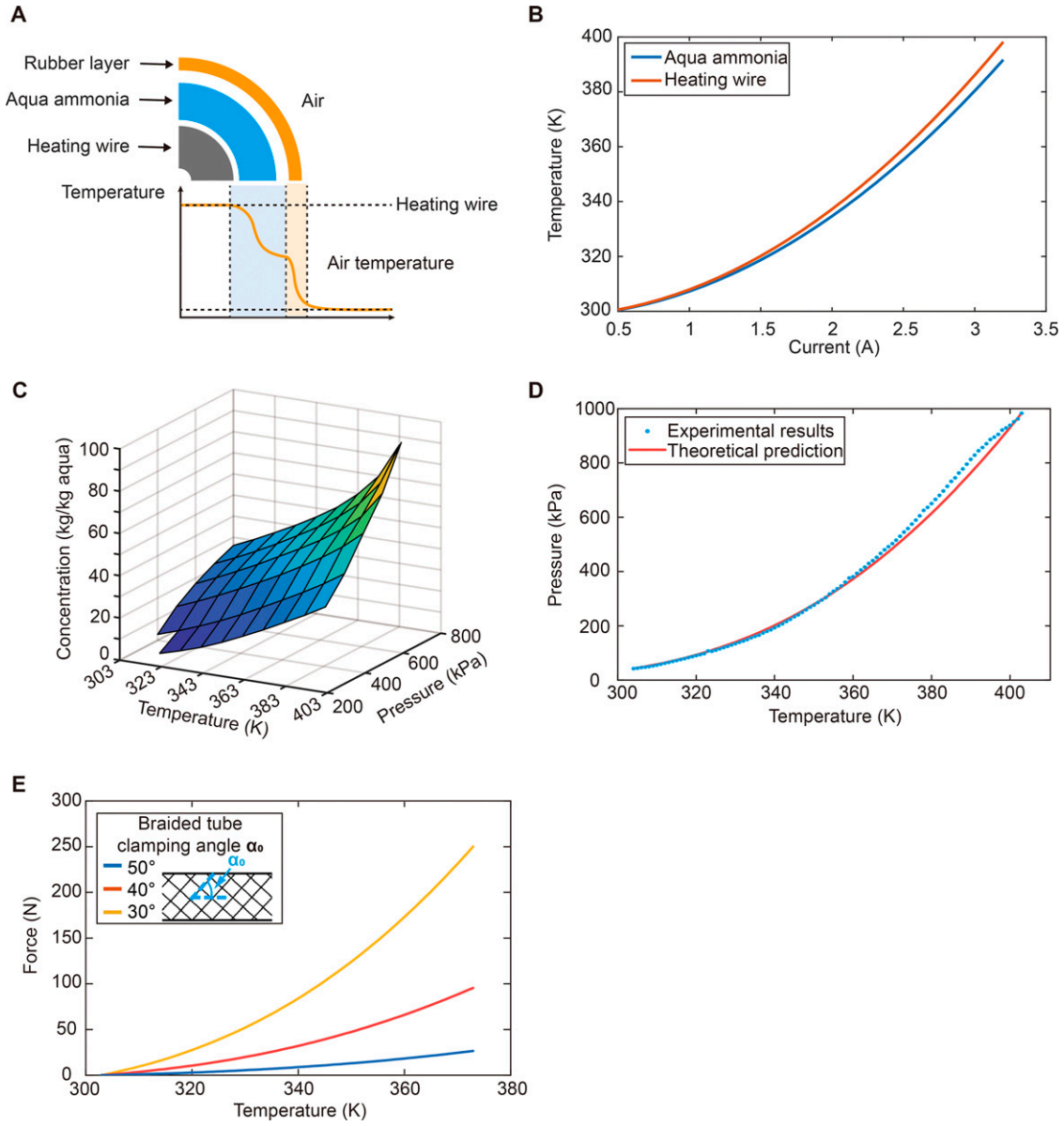


FIG. 2. Modeling and analysis. (A) The temperature distribution of the artificial muscle from the center to the surface. (B) Average stable temperature of aqua ammonia as a function of input current. (C) Concentration of aqua ammonia under different temperatures and pressures. (D) The gas pressure generated from aqua ammonia under different temperatures. (E) The artificial muscle's output force at different temperature.

second thermal resistance is the one in the heat convection between aqua ammonia and the inner wall of the rubber layer,

$$\Theta_2 = \frac{1}{h_{ammo}\pi d_{rin}}, \quad (7)$$

where d_{rin} is the diameter of the rubber layer's inner wall. The thermal resistance of the rubber layer,

$$\Theta_3 = \frac{1}{2\pi\lambda} \ln \frac{d_{ro}}{d_{rin}}, \quad (8)$$

where λ is the heat conduction coefficient of rubber and d_{ro} is the diameter of the outside of the rubber. The fourth thermal resistance is the heat convection between the rubber layer and air. Assuming the temperature of the air is constant,

$$\Theta_4 = \frac{1}{\alpha_{air}\pi r_{ro}}, \quad (9)$$

where α_{air} is the convection heat transfer coefficient of air. Thus, the heat loss is

$$Q_l = \frac{T_{core} - T_{\infty}}{\Theta} l, \quad (10)$$

where T_{core} is the temperature of the heating wire, T_{∞} is the temperature of the air, and l is the length of the actuator.

The heat generated by the heating wire is also used to heat aqua ammonia to make the aqua ammonia temperature rise, and the heat required to make the aqua ammonia change temperature can be expressed as follows:

$$Q_w = cm\Delta T, \quad (11)$$

where c is the specific heat capacity of the aqua ammonia, m is the mass of the aqua ammonia, and ΔT is the aqua ammonia's temperature change.

The heat required for the aqua ammonia decomposition reaction can be expressed as follows:

$$Q_r = \Delta Hn, \quad (12)$$

where ΔH is the reaction enthalpy of the decomposition reaction of aqua ammonia (24.01 kJ/mol^{53,54}), and n is the amount of ammonia produced by the reaction.

The amount of ammonia produced by the reaction can be obtained from the ideal gas law, which can be expressed as follows:

$$n = \frac{p_1 V_1}{RT_1} - \frac{p_0 V_0}{RT_0}, \quad (13)$$

where p_1 is the current air pressure, V_1 is the current gas volume, T_1 is the current temperature, p_0 is the initial air pressure, V_0 is the initial gas volume, T_0 is the initial temperature, and R is the gas constant [8.314 J/(mol·K)⁵⁵].

Based on the above equations, as shown in Figure 2B, the stable temperature exponentially increases with the current, and the temperatures of the heating wire and aqua ammonia fluid are almost the same. In the estimation, the initial resistance of the wire is 2 Ω , according to our prototype in the experiments.

Pressure generation of aqua ammonia

Ammonia in the solution system is present in the form of ammonia molecules and ammonium salt ions simultaneously in an amount of aqua ammonia. When heat flows into the aqua ammonia system, the balance of hydration and dissolution of ammonia molecules in the ammonia system is changed, and more ammonia gas is released. As shown in Figure 2C, as the temperature increases, more ammonia gas is generated due to the following chemical reaction:



Higher temperatures result in more ammonia gas in the air (due to more ammonia gas generated from the chemical reaction and the lower dissolution of ammonia in water) and more water vapor. Consequently, it leads to a higher pressure in a closed container.

Although ammonia gas is weakly toxic, leakage barely occurs for this well-sealed aqua ammonia system by a silicone layer. Even considering the severest theoretical situation when all produced gas is leaked to the external environment. Humans are in danger when exposed to a 50 ppm ammonia gas concentration environment,^{56,57} but the calculated peak value is only 21.59 ppm in a $5 \times 5 \times 3$ m confined space and quickly drops since ammonia gas does not accumulate in a ventilated environment such as the open or semi-open scenarios in demonstrations. Moreover, unlike odorless Novec 7000 that are typically used in previous actuators,^{15,29} the pungent odor of ammonia gas can alert for accidental leakage occurrence. Many methods have been developed to calculate the vapor-liquid equilibrium of a gas dissolution system. Previously, the

most widely used formula was Henry's law,⁵⁸ but it cannot accurately describe the gas that undergoes hydration and dissociation reactions (e.g., H₂S and NH₃). Here, we select the nonrandom two-liquid method⁵⁹ to build the analysis model. For a multicomponent system, the partial pressure, and the total pressure can be calculated by the following equation:

$$P_{total} = \sum P_i = \sum P_i^o x_i \gamma_i, \quad (15)$$

where P_i is the partial pressure of component i , γ_i is the activity coefficient of component i , and P_i^o is the saturated vapor pressure of component i , which is described by the Antoine function⁶⁰

$$\lg p_i^o = A - \frac{B}{T + C}, \quad (16)$$

where A, B, and C are the fitted coefficients, which can be acquired by experiments, and T is the temperature of the system. For a system of two substances, the activity coefficient can be written by the following equation:

$$\ln(\gamma_1) = x_2^2 \left[\tau_{21} \left(\frac{G_{21}}{x_1 + x_2 G_{21}} \right)^2 + \frac{G_{12} \tau_{21}}{x_2 + x_1 \tau_{12}} \right], \quad (17)$$

$$\ln(\gamma_2) = x_1^2 \left[\tau_{12} \left(\frac{G_{12}}{x_2 + x_1 G_{12}} \right)^2 + \frac{G_{21} \tau_{12}}{x_1 + x_2 \tau_{21}} \right], \quad (18)$$

where x_i is the liquid mole fraction of component i , and we have,

$$G_{12} = \exp(-\theta \tau_{12}), \quad (19)$$

$$G_{21} = \exp(-\theta \tau_{21}), \quad (20)$$

$$\tau_{12} = \frac{g_{12} - g_{22}}{RT}, \quad (21)$$

$$\tau_{21} = \frac{g_{21} - g_{11}}{RT}, \quad (22)$$

where G_{ij} and τ_{ij} are interactive coefficients and interactive energy between components i and j , and g_{ij} are the parameters for interaction between components i and j ($g_{ij} = g_{ji}$).

The above model is verified by the experimental results, as shown in Figure 2D, in which the theoretical results are calculated by equation (16). The parameters, A, B, and C of the Antoine equation are 4.90, 453.67, and -165.42, respectively, according to our preliminary trials. Thus, by controlling the temperature, heating, and cooling, we can control the direction of the aqua ammonia reaction and, therefore, the air pressure (Supplementary Fig. S1).

Actuation

The pressured gas inflates the soft actuator, consequently generating force and motion. The output force and motion depend on various specifications of the soft actuators, such as the volume, the material elasticity, and the shape of the soft actuators.

Here, we build the model based on the form of the McKibben actuator as an example. The relationship between the actuator's output and internal air pressure at its initial length can be derived as follows⁶¹:

$$F_d = \pi \left(\frac{r_0}{\sin \alpha_0} \right)^2 P [3 \cos^2 \alpha_0 - 1] - (\pi r_0^2 P) \left[2h_0 \frac{(2 \cos^2 \alpha_0 (1 - \varepsilon)^2 - 1)}{(1 - \varepsilon)(1 - \cos^2 \alpha_0 (1 - \varepsilon)^2)} \right] \quad (23)$$

where F_s is the output force of the McKibben actuator, P is the internal gas pressure, r_0 is the initial radius of the actuator, α_0 is the initial angle of the braided tube grid, and h_0 is the ratio of the initial shell thickness and radius ($h_0 = t_0/r_0$). Based on this equation, we can find that the output force exponentially rises with the air pressure. Meanwhile, the air pressure increases as the temperature rises. The output force rises with the temperature, as shown in Figure 2E. In this estimation, the radius r_0 is 6 mm, and h_0 is 0.1, which corresponds to the prototypes used in this work. Meanwhile, the diameters can also affect the output force of the artificial muscle according to the formula. All these parameters are fixed in the force experiments to eliminate the effect of the parameters.

Fabrication and Assembly

The fabrication of the actuator prototype is shown in Figure 3. First, two ends of the heating wire made from nickel-chromium alloy (length: 200 mm and diameter: 0.35 mm) were wound on two bolts, respectively. Then, the heating wire was inserted into a rubber tube (thickness: 0.15 mm; length: 200 mm; outer diameter: 10 mm). This rubber tube was then covered by a braided tube (10 mm diameter). After being injected with aqua ammonia (mass concentration 25%, Shanghai Titan Scientific Co., Ltd), the two ends of the rubber tube were tightly bound by straps. Finally, the heating wires were connected to the electrical power source and ready for actuation.

With the aqua ammonia, we also made a pouch actuator. To create it, we first folded a thermoset film (polyethylene [PE]). Then, we pressed and heated the edge of the thermoset film and finally made a pouch into which we injected aqua ammonia.

Experimental Results

Characterization

(A) Air pressure generated by aqua ammonia. To compare the pressure generated by aqua ammonia, ethanol, and water, we conducted experiments with the setup shown in Supplementary Figure S2A. As shown in Figure 4A, the pressure generated by the decomposition of aqua ammonia (mass concentration 25%, Shanghai Titan Scientific Co., Ltd.) increases significantly. It is 10 times higher than that of ethanol (mass concentration 99.7%, Shanghai Titan Scientific Co., Ltd.) vapor pressure in the low-temperature region (<323 K) and 2.5 times higher in the higher-temperature region (more than 373 K, higher than ethanol boiling point of 351.5 K³⁰), respectively. Ethanol is a typical substance for phase transition in the

previous electrical-driven soft actuators.^{30,32,48} The results also indicate that water vaporization partly contributes to the increase in pressures for this aqua ammonia system. The visualized comparison in Supplementary Video S1 and Figure 4B exhibits a larger expansion rate and size of a balloon encapsulating aqua ammonia heated by silicone oil (PMX-200, Shanghai Aladdin Biochemical Technology Co., Ltd.) under different temperatures than that of a balloon inflated by ethanol vapor from the same volume of solution.

(B) Contraction distance and velocity. We fixed one end and freed the other to measure the contraction velocity of the artificial muscle (200 mm in length and 10 mm in diameter). The artificial muscle shrunk by supplying the artificial muscle with a constant current of 1–3 A, and the free end's displacement was acquired by a laser displacement sensor (Panasonic HG-C1100).

The contraction distance increased almost linearly during the heating process, as shown in Supplementary Figure S3, which can benefit the control of the actuator. The contraction velocity rises, and the response time decreases with a higher current. The maximum contraction velocity reaches 2.95 mm/s when the current of 3 A is applied (Fig. 4C), comparable with other phase transition-based actuators^{17,30,47,48} (Supplementary Table S1). Since a constant voltage source, for example, batteries, is frequently used to drive the actuator in practical applications, we also compare the contraction velocity of the artificial muscle under different voltages in Supplementary Figure S4. Similar to the current, the contraction velocity of the artificial muscle increases, and the response time decreases with the increase in voltage. Actuator with a fast velocity and a quick response can be fulfilled by applying a higher current or voltage. However, it should be noted that a large current may cause a fuse to the heating wire, resulting in the failure of the actuator.

(C) Force. To measure the output force, the artificial muscle (150 mm in length and 10 mm in diameter) was fixed on the two ends, one of which was connected to a load cell (ZNLBS-20kg) (Supplementary Fig. S2B). Figure 4D characterizes the mechanical behaviors of a McKibben actuator filled with aqua ammonia under a constant current of 2 A, including a linear increase of output force up to approximately 10 N within 20 s at first, followed by a slow force growth in the next minute, and finally breaks down due to the melting of the silicone encapsulation layer where 18 N is recorded. In practice, the linear growth portion of the first 20 s can be used for force output, and the actuator's force output is more stable during this interval. As predicted in the aforementioned model, the output force of the artificial muscle is determined by and increases with the applied current. On another McKibben actuator made by the same parameters, a maximum output force of 43.6 N under 5 A was measured after 20 s actuation. Figure 4E shows good agreement between theoretical predictions and experimental results. A peak value of the artificial muscle in this work occurred in the demonstration, which is 49 N, 550 times its self-weight (8.9 g).

The pouch actuator, as a simple actuator, is a fundamental building block of many artificial muscles and can also function as a stand-alone one in many scenarios^{17,49} Hence, it is a perfect paradigm to illustrate the powerful force output

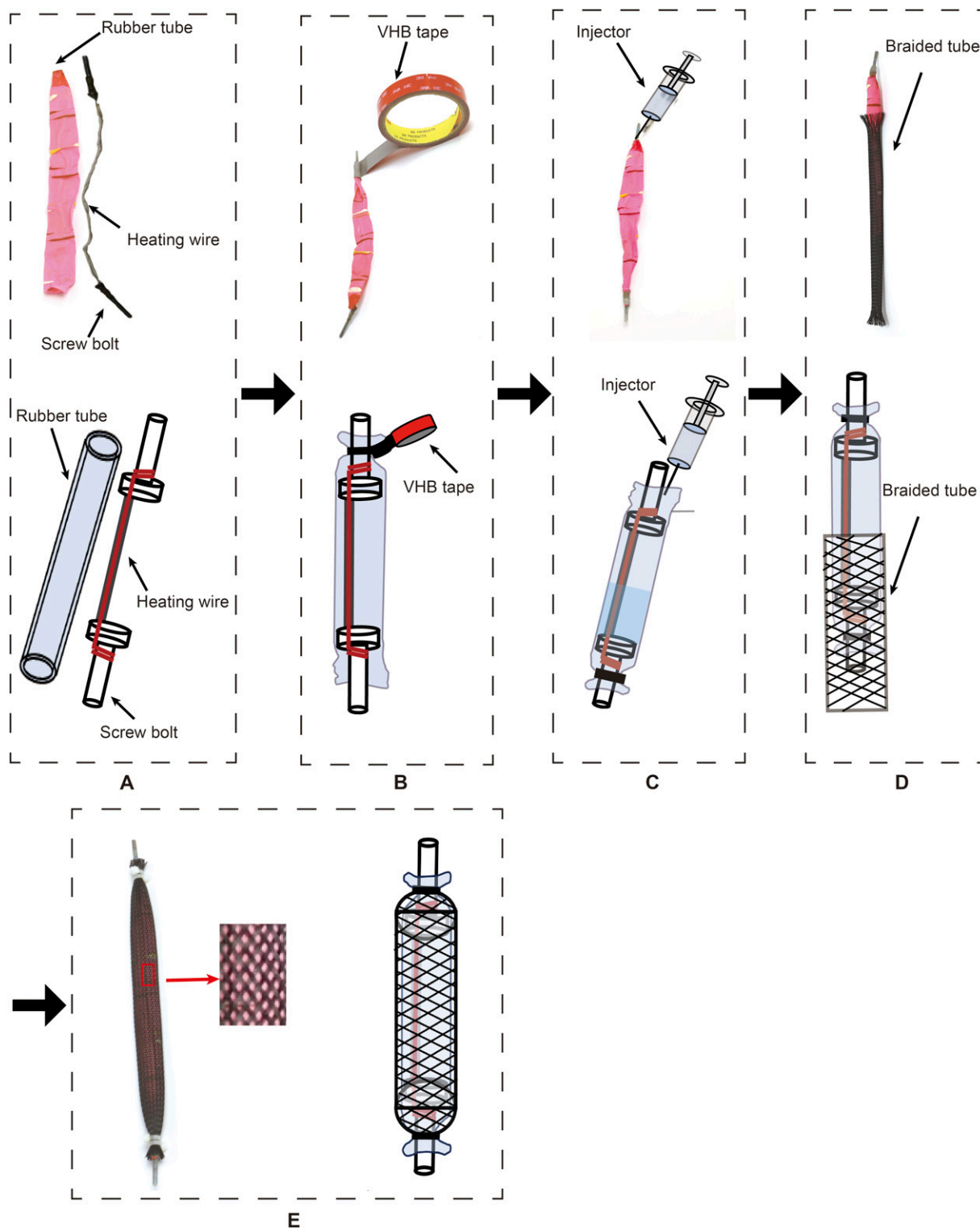


FIG. 3. Fabrication process of the McKibben artificial muscle. **(A)** Connecting the wires to two bolts. **(B)** Inserting the heating wire into the rubber tube and fastening one side by tape. **(C)** Injecting aqua ammonia into the rubber tube. **(D)** Covering the artificial muscle with a braided tube. **(E)** Fixing the braided tube and connecting the wires to power suppliers for actuation.

capabilities driven by the aqua ammonia system. Currently, the maximum output force was found on a pouch actuator (3.6 g, 100 mm in length, 100 mm in width) made from PE films (0.1 mm thick) filled with aqua ammonia. Driven by an

electric heater, the pouch actuator inflates and pushes against a force sensor of a testing machine (MTS Criterion Model C42). The recorded maximum output force is nearly 740 N, 20,555 times its deadweight (Supplementary Fig. S5), which

outperforms other counterparts^{4,15,26,30,33,50} and three times in force density of the previous work³⁰ (Fig. 1A).

(D) **Size.** To investigate the size effect on the output force and contraction distance of the artificial muscle, three different lengths, 100, 150, and 200 mm, of artificial muscles with the same radius were fabricated, filled with aqua ammonia of 40% of the initial volume of the latex tube. As shown in Figure 4F, as the length of the artificial muscle increases, its contraction distance increases accordingly, and the contraction rate is about 15–20% of the length. The output force of the artificial muscle did not show a significant increase with length, which can be explained by equation (23), indicating that length does not affect the output force of the McKibben artificial muscle.

(E) **Power.** To calculate the power consumption, a constant current of 1–3 A was supplied to the artificial muscle (150 mm in length and 10 mm in diameter) for 10 s, and the actual voltage applied to the artificial muscle was measured as shown in Figure 4G. The power consumption is approximately proportional to the square of the input current. The highest calculated power in 10 s is 19.946 W under 3 A actuation for the heating wire (2 Ω). The fluctuation in power is due to the rapid contraction of the artificial muscle causing instability in the resistance value of the heating wire.

(F) **Repeatability.** Moreover, we measured the repeatability of the soft artificial muscle with the same setup. As shown in Figure 4H, powered by a periodic 2 A current (20 s on, 40 s off), the artificial muscle (165 mm in length and 10 mm in diameter) displayed a stable movement with a period of 60 s for 48 cycles.

Demonstration

Two demonstrations display the various applications of the chemical principle. First, a McKibben artificial muscle (8.9 g) embedded with the aqua ammonia (3 g, 25%) and a heating wire lifted a weight of 5 kg while shrinking 5% of its initial length (24 cm) within 40 s under the electrical input of 10 V, 2.5 A, as shown in Figure 5A and Supplementary Video S2. The force/weight ratio is 5505.1 N/kg.

We also created a pouch actuator (3.179 g, 100 mm long, and 95 mm wide) made from PE films (0.1 mm thickness) and filled the pouch with aqua ammonia (1.5 g, 25%). When the pouch actuator was heated by an electric heater at the temperature of 337 K, it grew and lifted the weight (5 kg, force/weight ratio is 15408.8 N/kg) above it (Fig. 5B and Supplementary Video S3).

Next, we built an untethered soft robot, as shown in Figure 5C and Supplementary Video S4. The onboard power control circuit made in this work was placed on the actuator. For the mobile robots integrating the aqua ammonia actuator,

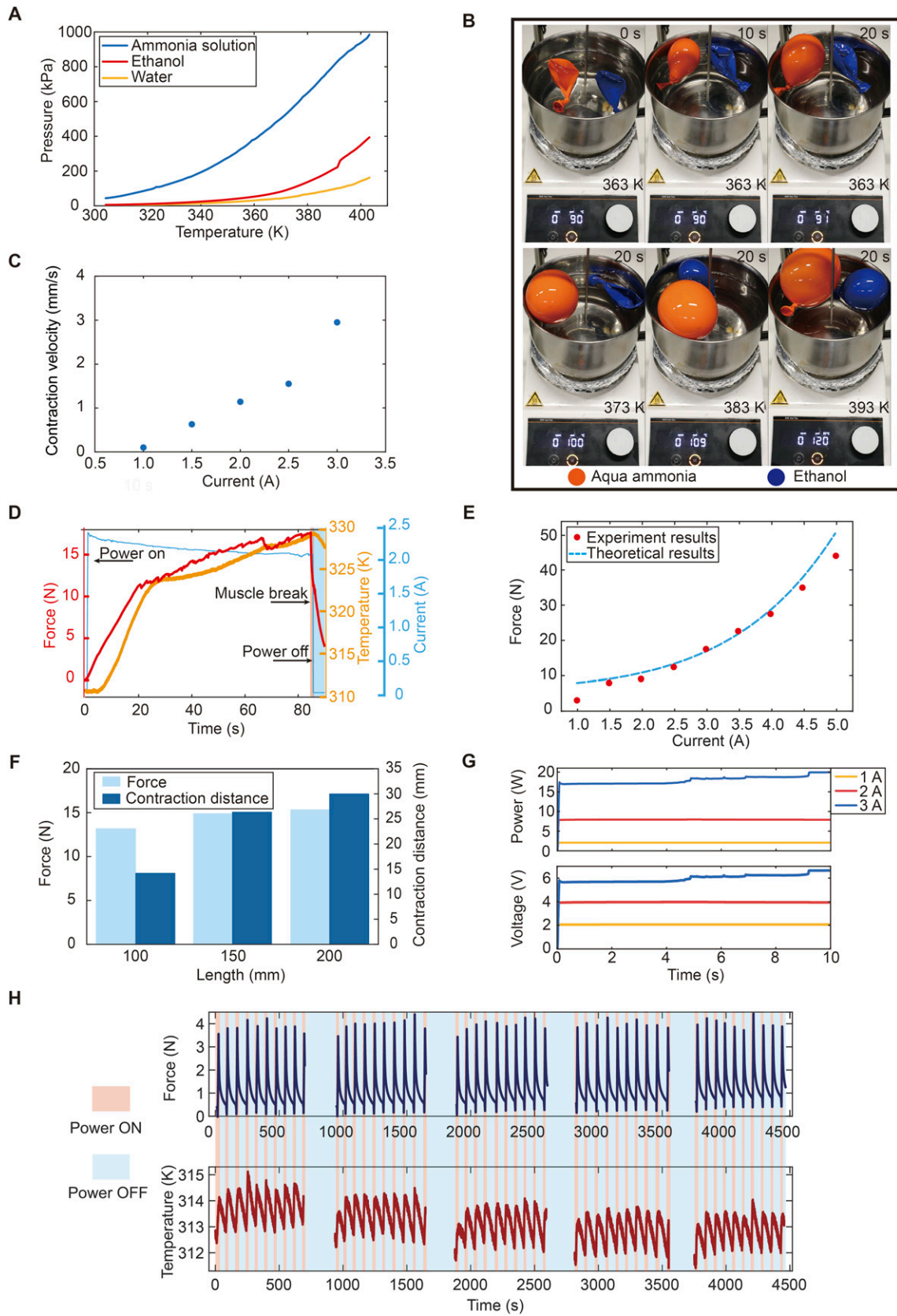
we designed a mobile power module for the untethered robotic application. A circuit that can drive the actuators simultaneously was designed for onboard driving. Three batteries (Panasonic 702535) connected in series powered the actuator, and a 9V battery (6F22) powered the control circuit. The heating wire in the actuator was connected to a high-power thyristor (Panasonic, AQV252G2S) in series. An onboard microcontroller (ATMEL, ATmega 328P) switched the electricity on the heating wire through the thyristors on and off. The weight of the mobile power module is 107 g. In each actuation cycle, the wire was powered on for about 10 s and then off for about 20 s. Correspondingly, the actuator shrank and expanded. Consequently, the robot moved successfully.

Conclusion

This work proposes to inflate the pneumatic actuators by the vapor pressure at the gas–liquid equilibrium of aqua ammonia. The models describing the energy conversion process from electrical energy are built and verified by experiments. Based on this mechanism, we fabricated several soft pneumatic actuators with aqua ammonia. Experimental results show that the vapor pressure increases with the temperature and the actuation voltage. Higher voltage and larger current result in larger velocity and stronger output force. Powered on and off in order, the actuator embedded with heating wires shrinks and expands, correspondingly, and this working cycle can be repeated more than 50 times. With aqua ammonia, the soft pouch actuator can push a load of more than 20,555 times heavier than its own weight. Finally, we demonstrate an untethered soft crawling robot that moves freely without any pipelines connected to pumps (common to previous soft pneumatic robots), which integrates the soft actuator driven by the vapor pressure of aqua ammonia and onboard batteries and controllers.

However, the performance shown in this article does not fully demonstrate the performance of ammonia due to the limitations of the thermal material, and ammonia should be able to show even better results when higher power or more advanced heating methods are used. The chemical balance can be easily combined with optical and magnetic actuation, such as using pure flexible high-frequency oscillators to promote the decomposition of aqua ammonia, which may further improve the output effect while reducing energy loss. Safer and more efficient methods, such as the carbonic acid system, can be developed similar to the ammonia system. Meanwhile, since there is an accurate pressure–temperature relationship, the controllability of this new type of actuator would show a great advantage. In the future, pulse width modulation can be exploited to regulate the driving current for better onboard control to realize precise pressure actuation of soft robots.

FIG. 4. Experimental results of the artificial muscle driven by the vapor pressure of aqua ammonia. (A) Comparison of the vapor pressure generated from aqua ammonia, ethanol, and water in a closed container. (B) Comparison of the inflation of balloons filled with aqua ammonia and ethanol at different temperatures. (C) Contraction velocity of the artificial muscle at different currents. (D) The variance of the temperature, current, and output force during the artificial muscle operation. (E) The output force of the artificial muscle at different currents in 20 s. (F) Comparison of output force and contraction displacement for different lengths of the artificial muscles. (G) Input voltage and power consumption of the artificial muscle at different currents. (H) The repeatability of the artificial muscle (50 cycles).



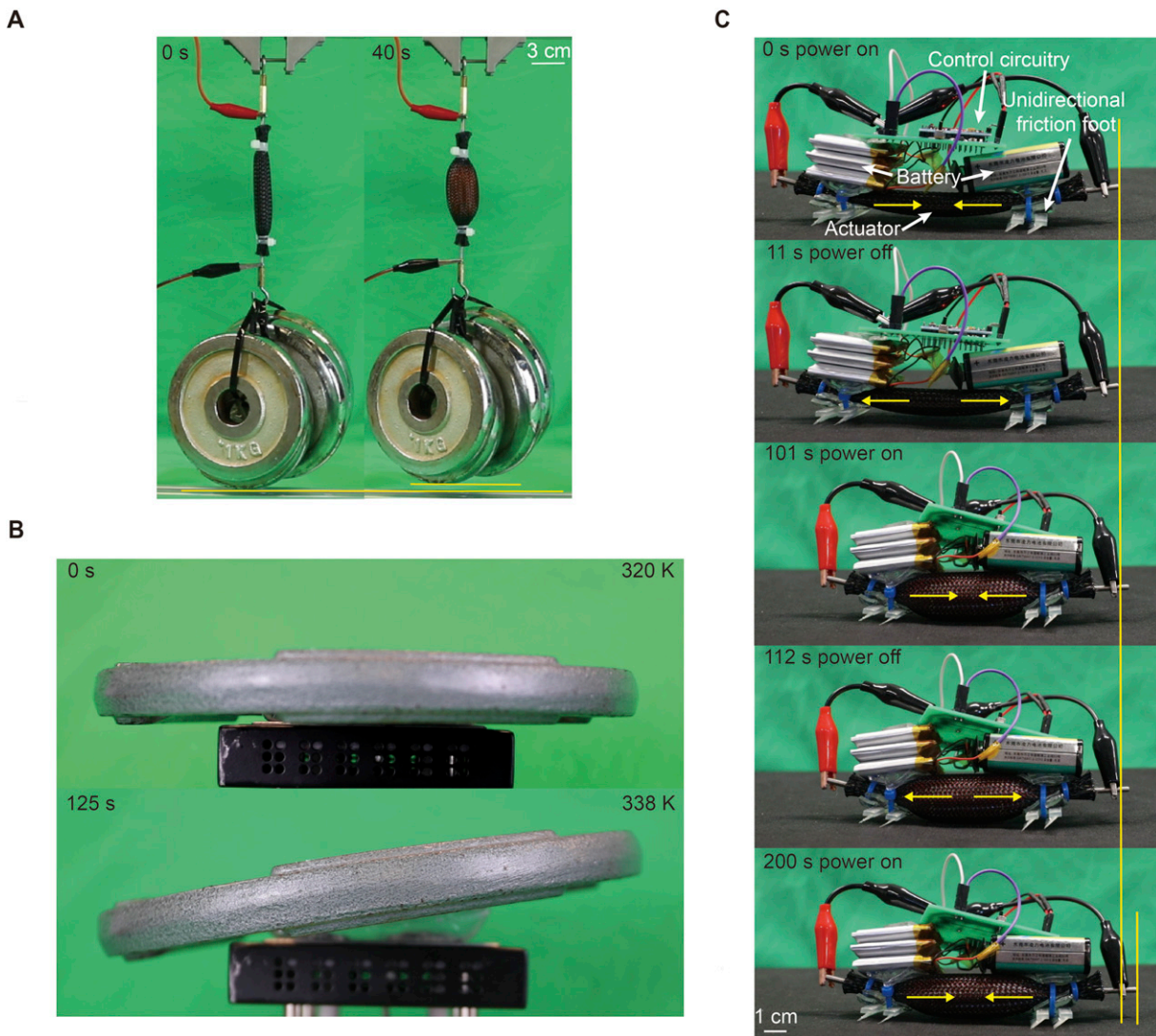


FIG. 5. Demonstration of the artificial muscle by heating aqua ammonia. (A) Pull up 5 kg weight. (B) Lift up 5 kg of weight. (C) Crawling demo of the artificial muscle.

Author Disclosure Statement

No competing financial interests exist.

Authors' Contributions

Y. Q. and H. W. (Hongqiang Wang) conceived the idea. Y. Q. and Y. Z. performed the experiments, derived the theoretical model, and developed the demonstrations. B. H. contributed to the experiments and data analysis. C. C. assisted with the experiments and manuscript revisions. H. W. (Huacen Wang) created the figures. S. L. supervised the experiments and provided guidance during manuscript revisions. H. W. (Hongqiang Wang) oversaw the project and contributed to drafting the manuscript. All authors reviewed and approved the final version of the manuscript.

Funding Information

This study was supported in part by the National Key R&D Program of China under Grant No. 2022YFB4701200, in part by the National Natural Science Foundation of China

under Grant No. 52275021, in part by the Science, Technology, and Innovation Commission of Shenzhen Municipality under Grant No. ZDSYS20200811143601004, in part by the Natural Science Foundation of Liaoning Province of China (State Key Laboratory of Robotics joint funding, under Grant No. 2021-KF-22-11), in part by Southern Marine Science and Engineering Guangdong Laboratory (Guangzhou) under Grant No. K19313901 and in part by Guangdong Provincial Research Support Program under Grant 2019QN01Z733.

Supplementary Material

Supplementary Figure S1
 Supplementary Figure S2
 Supplementary Figure S3
 Supplementary Figure S4
 Supplementary Figure S5
 Supplementary Table S1
 Supplementary Video S1
 Supplementary Video S2

Supplementary Video S3
Supplementary Video S4

References

- Rich SI, Wood RJ, Majidi C. Untethered soft robotics. *Nat Electron* 2018;1(2):102–112.
- Wu Y, Liu M, Zhang G, et al. Study on high frequency response characteristics of a moving-coil-type linear actuator using the coils combinations. *IJHM* 2022;5(3):226–242.
- Xiang P, Yan L, Guo Y, et al. A concentrated-flux-type pm machine with irregular magnets and iron poles. *IEEE/ASME Trans Mechatron* 2024;29(1):691–702.
- Tolley MT, Shepherd RF, Mosadegh B, et al. A resilient, untethered soft robot. *Soft Robotics* 2014;1(3):213–223.
- Fan D, Yuan X, Wu W, et al. Self-shrinking soft demoulding for complex high-aspect-ratio microchannels. *Nat Commun* 2022;13(1):5083.
- Li D, Fan D, Zhu R, et al. Origami-inspired soft twisting actuator. *Soft Robot* 2023;10(2):395–409.
- Zou J, Lin Y, Ji C, et al. A reconfigurable omnidirectional soft robot based on caterpillar locomotion. *Soft Robotics* 2018;5(2):164–174.
- Jiao Z, Zhang C, Wang W, et al. Advanced artificial muscle for flexible material-based reconfigurable soft robots. *Adv Sci (Weinh)* 2019;6(21):1901371.
- Ge L, Chen F, Wang D, et al. Design, modeling, and evaluation of fabric-based pneumatic actuators for soft wearable assistive gloves. *Soft Robotics* 2020;7(5):583–596.
- Wehner M, Truby RL, Fitzgerald DJ, et al. An integrated design and fabrication strategy for entirely soft, autonomous robots. *Nature* 2016;536(7617):451–455.
- Wang H, York P, Chen Y, et al. Biologically inspired electrostatic artificial actuators for insect-sized robots. *The International Journal of Robotics Research* 2021;40(6–7):895–922.
- Tolley MT, Robert SF, Michael K, et al. An untethered jumping soft robot. In: *IEEE/RSJ International Conference on Intelligent Robots and Systems*. IEEE; 2014;561–566.
- Wang H, Akio Y, Higuchi T. Electrostatic-motor-driven electroadhesive robot. In: *IEEE/RSJ International Conference on Intelligent Robots and Systems*. IEEE; 2012;914–919.
- Cvetkovic C, Raman R, Chan V, et al. Three-dimensionally printed biological machines powered by skeletal actuator. *Proc Natl Acad Sci USA* 2014;111(28):10125–10130.
- Kang R, Guo Y, Chen L, et al. Design of a pneumatic muscle based continuum robot with embedded tendons. *IEEE/ASME Trans Mechatron* 2017;22(2):751–761.
- Ghafoor A, Dai JS, Duffy J. Stiffness modeling of the soft-finger contact in robotic grasping. *J. Mech. Des* 2004;126(4):646–656.
- Boyvat M, Vogt DM, Wood RJ. Ultrastrong and high-stroke wireless soft actuators through liquid-gas phase change. *Adv Materials Technologies* 2019;4(2):1800381.
- Lin Y, Zhang C, Tang W, et al. A bioinspired stress-response strategy for high-speed soft grippers. *Advanced Science* 2021;8(21):2102539.
- Hironari T. Flexible artificial actuator using coiled shape memory alloy wires. *APCBEE Procedia* 2013;7:54–59.
- Bhandari B, Lee GY, Ahn SH. A review on IPMC material as actuators and sensors: Fabrications, characteristics and applications. *Int J Precis Eng Manuf* 2012;13(1):141–163.
- Nguyen CT, Phung H, Nguyen TD, et al. Multiple-degrees-of-freedom dielectric elastomer actuators for soft printable hexapod robot. *Sensors and Actuators A-Physical* 2017;267:505–516.
- Kunze J, Precht J, Bruch D, et al. Design, manufacturing, and characterization of thin, core-free, rolled dielectric elastomer actuators. *Actuators*. MDPI 2021;10:69.
- Wei D, Xiong Q, Dong J, et al. Electrostatic adhesion clutch with superhigh force density achieved by mxene-poly (vinylidene fluoride–trifluoroethylene–chlorotrifluoroethylene) composites. *Soft Robotics* 2023;10(3):482–492.
- Xie G, Fan D, Wang H, et al. Strong reliable electrostatic actuation based on self-clearing using a thin conductive layer. *Soft Robot* 2023;10(4):797–807.
- Qian P, Liu L, Pu C, et al. Methods to improve motion servo control accuracy of pneumatic cylinders-review and prospect. *IJHM* 2023;6(3):274–310.
- Lee JG, Rodrigue H. Origami-based vacuum pneumatic artificial actuators with large contraction ratios. *Soft Robot* 2019;6(1):109–117.
- Polygerinos P, Wang Z, Galloway KC, et al. Soft robotic glove for combined assistance and at-home rehabilitation. *Robotics and Autonomous Systems* 2015;73:135–143.
- Drotman D, Jadhav S, Sharp D, et al. Electronics-free pneumatic circuits for controlling soft-legged robots. *Sci Robot* 2021;6(51):eaay2627.
- Chen Y, Wang H, Helbling EF, et al. A biologically inspired, flapping-wing, hybrid aerial-aquatic microrobot. *Science Robotics* 2017;2:eaay5619.
- Miriyev A, Stack K, Lipson H. Soft material for soft actuators. *Nat Commun* 2017;8(1):596.
- Nakahara K, Narumi K, Niiyama R, et al. Electric phase-change actuator with inkjet printed flexible circuit for printable and integrated robot prototyping. 2017 *IEEE International Conference on Robotics and Automation (ICRA)*. IEEE; 2017; 1856–1863.
- Long F, Cheng Y, Ren Y, et al. Latest advances in development of smart phase change material for soft actuators. *Adv Eng Mater* 2022;24(3):2100863.
- Li H, Yao J, Zhou P, et al. High-load soft grippers based on bionic winding effect. *Soft Robot* 2019;6(2):276–288.
- Tawk CY. 3D printed pneumatic soft actuators and sensors: their modeling, performance quantification, control and applications in soft robotic systems. Doctor of Philosophy thesis, School of Mechanical, Material, Mechatronic and Biomedical Engineering, University of Wollongong, 2019.
- Park YL, Santos J, Galloway KG, et al. A soft wearable robotic device for active knee motions using flat pneumatic artificial actuators. 2014 *IEEE International Conference on Robotics and Automation (ICRA)*, 2014;4805–4810.
- Moseley P, Florez JM, Sonar HA, et al. Modeling, design, and development of soft pneumatic actuators with finite element method. *Adv Eng Mater* 2015;18(6):978–988.
- Wang Z, Polygerinos P, Overvelde JTB, et al. Interaction forces of soft fiber reinforced bending actuators. *IEEE/ASME Trans Mechatron* 2017;22(2):717–727.
- Guo J, Sun Y, Liang X, et al. Design and fabrication of a pneumatic soft robotic gripper for delicate surgical manipulation. 2017 *IEEE International Conference on Mechatronics and Automation (ICMA)*. IEEE; 2017;1069–1074.
- Guo XY, Li WB, Gao QH, et al. Self-locking mechanism for variable stiffness rigid–soft gripper. *Smart Mater Struct* 2020;29(3):35033.

40. Laura P, Gunjan A, Jamie P. Design and analysis of a soft pneumatic actuator with origami shell reinforcement. *Soft Robotics* 2016;3:109–119.
41. Li X, Chen Y, Yang Y, et al. Passive particle jamming and its stiffening of soft robotic grippers. *IEEE Trans Robot* 2017;33(2):446–455.
42. Xie Z, Domel AG, An N, et al. Octopus arm-inspired tapered soft actuators with suckers for improved GraspIn. *Soft Robot* 2020;7(5):639–648.
43. Santoso J, Cagdas DO. An origami continuum robot capable of precise motion through torsionally stiff body and smooth inverse kinematics. *Soft Robot* 2021;8(4):371–386.
44. Cheng NG, Lobovsky MB, Keating SJ, et al. Design and analysis of a robust, low-cost, highly articulated manipulator enabled by jamming of granular media. 2012 IEEE international conference on robotics and automation. IEEE, 2012; 4328–4333.
45. Li H, Yao J, Zhou P, et al. High-force soft pneumatic actuators based on novel casting method for robotic applications. *Sens Actuators A: Physi* 2020;306:111957.
46. Hu W, Mutlu R, Li W, et al. A structural optimisation method for a soft pneumatic actuator. *Robotics* 2018;7(2):24.
47. Chellattoan R, Yudhanto A, Lubineau G. Low-voltage-driven large-amplitude soft actuators based on phase transition. *Soft Robot* 2020;7(6):688–699.
48. Han J, Jiang W, Niu D, et al. Untethered soft actuators by liquid–vapor phase transition: Remote and programmable actuation. *Adva Intelli Systems* 2019;1(8):1900109.
49. Meder F, Naselli GA, Sadeghi A, et al. Remotely light-powered soft fluidic actuators based on plasmonic-driven phase transitions in elastic constraint. *Advan Materi* 2019;31(51):1905671.
50. Shao Y, Long F, Zhao Z, et al. 4D printing light-driven soft actuators based on liquid-vapor phase transition composites with inherent sensing capability. *Che Engi J* 2023;454:140271.
51. Ulanowicz RE. Mass and energy flow in closed ecosystems. *J Theor Biol* 1972;34(2):239–253.
52. Mirvakili SM, Sim D, Hunter IW, et al. Actuation of untethered pneumatic artificial muscles and soft robots using magnetically induced liquid-to-gas phase transitions. *Sci Robot* 2020;5(41):eaaz4239.
53. Fortes AD, Brodholt JP, Wood IG, et al. Ab initio simulation of ammonia monohydrate ($\text{NH}_3 \cdot \text{H}_2\text{O}$) and ammonium hydroxide (NH_4OH). *J Chem Phys* 2001;115(15):7006–7014.
54. Brown TL. *Chemistry: The Central Science*. Pearson Education; 2009.
55. Moran MJ, Shapiro HN, Boettner DD, et al. *Fund Engin Thermodynamics*. John Wiley & Sons; 2010.
56. Roney N, Llados F. Toxicological profile for ammonia. 2004.
57. Jiao Y, Niu L, Ma S, et al. Quaternary ammonium-based biomedical materials: State-of-the-art, toxicological aspects and antimicrobial resistance. *Prog Polym Sci* 2017;71:53–90.
58. Mackay D, Shiu WY. A critical review of Henry's law constants for chemicals of environmental interest. *J Phys Chem Reference Data* 1981;10(4):1175–1199.
59. Darde V, Thomsen K, van Well WJM, et al. Comparison of two electrolyte models for the carbon capture with aqueous ammonia. *Inter J Greenhouse Gas Control* 2012;8:61–72.
60. Rodgers RC, Hill GE. Equations for vapour pressure versus temperature: Derivation and use of the antoine equation on a hand-held programmable calculator. *Br J Anaesth* 1978; 50(5):415–424.
61. Tondu B. Modelling of the McKibben artificial actuator: A review. *Journal of Intelligent Material Systems and Structures* 2012;23(3):225–253.

Address correspondence to:

Hongqiang Wang
Shenzhen Key Laboratory of Biomimetic Robotics and
Intelligent Systems
Department of Mechanical and Energy Engineering
Southern University of Science and Technology
No. 1088
Xueyuan Blvd.
Xili
Nanshan District
Shenzhen
Guangdong 518055
China

E-mail: wanghq6@sustech.edu.cn